RSC Advances

PAPER

View Article Online
View Journal | View Issue

Cite this: *RSC Adv.*, 2025, **15**, 36760

Wool-supported Pd and Rh nanoparticles for selective hydrogenation of maleic acid to succinic acid in batch and flow systems

Francesca Coccia, [ab] Andrea Mascitti,[c] Stefano Caporali, [d] Laura Polito,[e] Andrea Porcheddu, [f] Corrado Di Nicola, [g] Lucia Tonucci [*ah] and Nicola d'Alessandro [bhi]

Received 24th July 2025
Accepted 29th September 2025

DOI: 10.1039/d5ra05365j

rsc.li/rsc-advances

Wool fibers, a renewable and biodegradable waste material, provide an eco-friendly platform for supporting metal nanoparticles, thanks to their unique amino acid composition. This study reports a fast and straightforward synthesis of palladium and rhodium nanoparticles (Pd and Rh NPs) supported on wool fibers (Pd NPs/WF and Rh NPs/WF) derived from low-grade wool. The resulting catalysts, with dispersed spherical nanoparticles (about 5 nm), were characterized by SEM, TEM, XPS, and XRD. They were tested for the selective hydrogenation of maleic acid (MA) to succinic acid (SA) under mild batch and continuous-flow conditions. Both catalysts exhibited excellent activity and full selectivity, achieving complete conversion in 2 h with 3 mol% metal loading in batch, in water solution at room temperature and under H_2 flux. Notably, Rh/WF also performed effectively in a fixed-bed flow reactor using hydrazine sulfate as an alternative hydrogen donor and fully converted MA into SA in 75 minutes, in a water solution at room temperature. The catalysts were robust and recyclable without loss of activity, highlighting wool-supported Pd and Rh NPs as sustainable and efficient catalysts for aqueous hydrogenation reactions.

Introduction

Heterogeneous catalysis is a cornerstone of chemical transformations, providing exceptional versatility and efficiency in numerous industrial processes. It enables the recycling and reuse of catalysts, reduces contamination and the need for purification steps, and allows continuous processing. Among several supports available, natural textile fibers, like wool or cotton, stand out as innovative and sustainable options.[1] Wool, with its amino acid structure, allows different attaching/deposition protocols for organic molecules,[2] metals, metal complexes or metal oxides,[3–6] microorganisms[7] and enzymes.[8,9]

The European Union boasts a significant sheep population, with approximately 59 million sheep in 2022;[10] raw wool is classified as "special waste", making its management problematic. In several Countries, it must be separately disposed of, posing challenges for waste management and environmental sustainability.[11] The low cost of sheep wool, coupled with the supply chain's interest in finding alternative uses and the potential ease of chemical coating protocols, makes repurposing this special waste an attractive option for supported catalysts.[12] Furthermore, the structure and the mechanical properties of wool fibers (WF) enable their use in chemical reactors of various sizes; cysteine and glutamic acid are two major amino acids, principally in the keratin of the WF.[13,14] The multifunctional structure of WF presents a versatile platform for connecting with other materials. The carboxyl and amine terminal groups of amino acids, particularly those located on the outermost layers of wool, known as the cuticle, can easily interact with supported materials.[15] It is essential to highlight that covalently bound lipids,[16] together with some specific amino acids, contribute to the hydrophobic nature of the wool surface.[17]

[a]*Department of Socio-Economic, Managerial and Statistical Studies, University "G. d'Annunzio" of Chieti-Pescara, Viale Pindaro 42, Pescara, Italy. E-mail: lucia.tonucci@unich.it*

[b]*UdA-TechLab Research Center, University "G. d'Annunzio" of Chieti-Pescara, Via dei Vestini 31, Chieti, Italy*

[c]*Department of Engineering and Geology, University "G. d'Annunzio" of Chieti-Pescara, Viale Pindaro 42, Pescara, Italy*

[d]*Department of Industrial Engineering, University of Florence, Via Di Santa Marta 3, Florence, Italy*

[e]*Istituto di Scienze e Tecnologie Chimiche "Giulio Natta", SCITEC – CNR, Via G. Fantoli 16/15, Milano, Italy*

[f]*Dipartimento di Scienze Chimiche e Geologiche, Università degli Studi di Cagliari, Cittadella Universitaria, SS554 bivio per Sestu, Monserrato, CA, Italy*

[g]*School of Science and Technology, Chemistry Section, University of Camerino, Camerino, Italy*

[h]*TEMA Research Center, University "G. d'Annunzio" of Chieti-Pescara, Via dei Vestini 31, Chieti, Italy*

[i]*Department of Science, University "G. d'Annunzio" of Chieti-Pescara, Via dei Vestini 31, Chieti, Italy*

WF possess a high surface area per unit mass (0.96 $m^2\ g^{-1}$) compared to other textile fibers;[18] this characteristic combined with the presence of S, N, O promoted the deposition/coordination of metals. This facilitates the formation of metal-wool complexes or other metal derivatives including zero-valent state, metal oxides, *etc.* Moreover, cysteine disulfuric bridges (or their reduced form, thiols) can interact with and facilitate the reduction of several metal ions[19] thereby producing innovative hybrid materials.[20] In last years, some examples of metal-based nanoparticles (NPs) on WF, like ferrite,[21] MnO_2,[4] Fe_3O_4,[22] Pd,[6] active as catalysts, were reported. Specifically, Ghadamgahi *et al.* used Pd NPs, prepared with WF as reducing and supporting agent, to catalyze the reduction of cyclohexene to cyclohexane under 28 bar of H_2 at 40 °C.[6]

In this context, flow chemistry presents an appropriate solution to further enhance catalyst stability and recyclability. Flow chemistry modernizes traditional chemical synthesis by allowing precise control over reaction parameters in continuous-flow systems. By continuously feeding chemical reagents into a reactor, packed with supported catalyst, and collecting products at the outlet, an alternative and sustainable methodology can be proposed. The packed column can be utilized over an extended period until catalyst exhaustion, promoting both efficiency and sustainability.

The flow setup enables the recycling of the catalyst without any separation steps from the reaction mixture, and no filtration or washing is required. This approach prevents any loss of catalyst and avoids contamination of the final product. Additionally, it enhances catalyst stability since the catalyst isn't subjected to mechanical stress from stirring.[23]

Over the past few years, our research group has dedicated significant efforts to developing a series of metal NPs using industrial waste materials, specifically lignin derivatives. By employing lignin sulfonate as both a reducing and stabilizing agent, we successfully synthesized palladium, platinum, ruthenium, and rhodium NPs. These metal NPs were fully characterized and tested as selective catalysts in various oxidation, reduction, hydrogenation, and cross-coupling reactions, showcasing their potential in sustainable chemistry applications.[24–29]

In the present study, Pd NPs and Rh NPs on WF (Pd NPs/WF and Rh NPs/WF), deriving from low-grade wool, were synthesized with an easy and fast protocol, obtaining new active hybrid materials as hydrogenation catalysts of maleic acid (MA) to succinic acid (SA). SA is an important intermediate in chemical industry, mainly for the polymers production, even for the preparation of biodegradable ones, akin poly(butylene succinate), because MA can be derived from biomass platforms.[30–32] This selective hydrogenation is not so simple since MA could be catalytically converted, *via* protonation, to its isomer, fumaric acid (FA), which, in water solution, could be hydrated to malic acid.[33] In literature, the use of Pd as catalyst for the reduction of MA was reported but, frequently, hydrogen pressure superior to 5 bar was necessary meanwhile increasing the temperature could promote the FA formation.[30,34–36] The activity of rhodium is known for C–H bond and for selective reduction of C=C, even if less reported in the case of MA hydrogenation.[24] In the past, even the influence of the support for the Pd catalysts was highlighted in the hydrogenation of MA; this consideration prompt us to prepare and test the Pd and Rh NPs supported on WF, a natural, abundant, renewable, biodegradable and economic alternative.

Building on our previous works, we conducted reduction reactions in aqueous solutions at room temperature and atmospheric pressure, employing batch or continuous-flow setups. These reactions were carried out under a hydrogen atmosphere or using hydrazine salts as chemical reducing agents.

Results

Two types of catalysts were prepared for each metal: one with a higher metal concentration (H-Pd NPs/WF and H-Rh NPs/WF) and one with a lower concentration (L-Pd NPs/WF and L-Rh NPs/WF).

The synthesis, based on published works,[24–29,37] was performed in an aqueous solution at 80 °C for 6 h, using Pd or Rh salts, formic acid, and low-grade WF smaller than 250 μm. The WF turned black with Pd and dark brown with Rh and remained dark-colored even after washing and drying steps; they were stable in air and light for at least 3 months. A control synthesis was performed without formic acid. In this case, the WF turned brown for both metals, and the aqueous solution retained some coloration at the end of the synthesis, suggesting the presence of residual metals in the solution. ICP analysis confirmed here the partial deposition of metal NPs on the WF (63–74%), demonstrating that formic acid was critical in achieving complete metal deposition and ensuring high catalyst quality. In the literature, several examples of NPs obtained through the metal ions reduction to zero-valent state by amounts of formic acid are present.[37]

Conversely, in the presence of formic acid, the deposition of the metals was quantitative (Table 1). NPs/WF prepared without formic acid will no longer be taken into account in this study.

The presence of metals on WF was observed by SEM analysis (Fig. 1). The initial low-grade wool appeared as regular cylindrical fibers with a medium diameter of 44 μm and a wrinkled surface with a scale-like structure, typical of wool (Fig. 1A).[1] In the Fig. 1(B and C), morphological changes of fibers surface, after the preparation of the catalysts, were visible: the surface appeared rougher with a quasi-regular metal coating of the treated WF.[19,38]

Elemental mapping (Fig. S1 and S2) showed the distribution along the fibers of main characteristic elements, such as C, O, N, and S, present in the original wool, and the confirmation of the nature of coating materials: Pd (Fig. 2, left) and Rh (Fig. 2, right). Even in the EDX spectra, the presence of Pd or Rh was confirmed (Fig. S3 and S4). The presence of palladium in L-Pd/WF and of rhodium in L-Rh/WF was confirmed (Fig. S5 and S6).

To characterize the composition and the crystallinity of metal core deposited on WF, XRD spectra were acquired. The patterns of NPs on wool exhibited crystalline state with a core of metals in both cases. Pd NPs diffractogram showed the zero-valent state of Pd, described by the peaks at 2θ 40.07°, 46.59°,

Table 1 Amounts of Pd or Rh detected by ICP analysis in aqueous solution (supernatant + washing waters) of the Pd and Rh NPs/WF preparation, in presence (Y) or not (N) of formic acid

Catalyst	Formic acid	Metal amount in synthesis (mg L^{-1})	Metal detected in solution (mg L^{-1})	Metal supported on WF (calculated %, w/w)
H-Pd NPs/WF	Y	1704.00	0.08	100.0
H-Pd NPs/WF	N	1704.00	619.00	63.7
L-Pd NPs/WF	Y	852.00	0.12	100.0
L-Pd NPs/WF	N	852.00	224.00	73.7
H-Rh NPs/WF	Y	1646.40	1.07	99.9
H-Rh NPs/WF	N	1646.40	523.00	68.2
L-Rh NPs/WF	Y	823.20	0.95	99.9
L-Rh NPs/WF	N	823.20	229.00	72.2

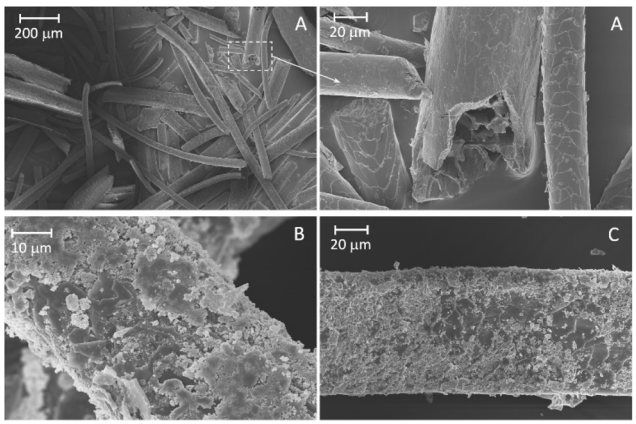

Fig. 1 SEM images of initial low-grade wool (A), H-Pd NPs/WF (B), H-Rh NPs/WF (C).

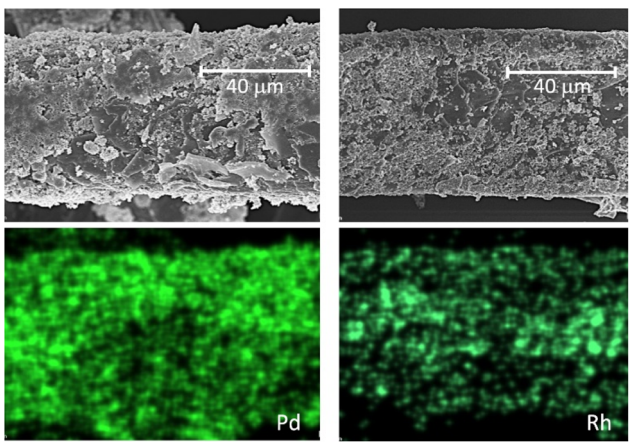

Fig. 2 Palladium and rhodium mapping (left, H-Pd/WF, right, H-Rh/WF).

68.07°, 82.06° and 86.76° (Fig. S7, left), assigned to diffraction of (111), (200), (220), (311) planes of the face-centered cubic metal crystal.[28,39] Even Rh NPs diffractogram showed the zero-valent state of Rh; its signals were at 2θ 41.14°, 47.86°, 70.00°, 84.23° and 89.1°, corresponding to the (111) (200), (220), (311) and (222) planes of Rh (Fig. S7, right).[40]

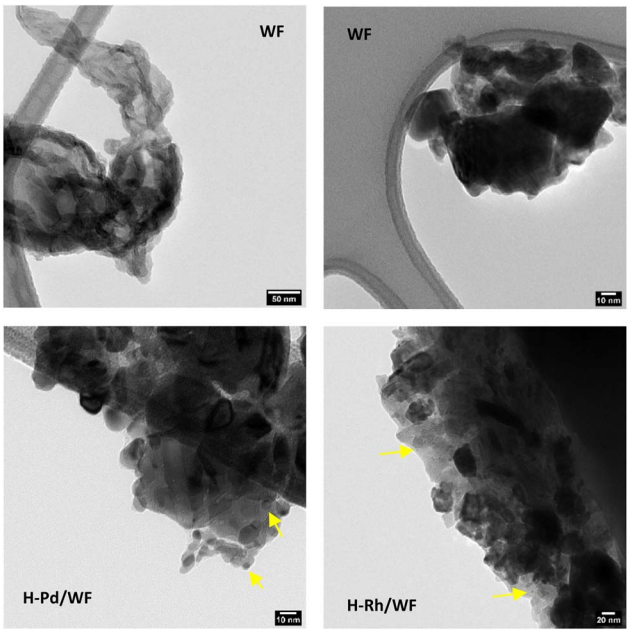

Fig. 3 TEM micrographs of WF (upper), H-Pd/WF (bottom, left), and H-Rh/WF (bottom, right).

The presence of metal NPs has been demonstrated also by TEM micrographs. As reported in Fig. 3, Pd (bottom, left) and Rh (bottom, right) spherical NPs were visible and embedded in the WF. The diameter for H-Pd NPs was estimated to be 5.0 ± 1.3 nm, while for H-Rh NPs the medium size was centered at 5.6 ± 1.5 nm (Fig. 4). The L-Pd and L-Rh were similar or smaller (5.3 ± 1.2 and 4.9 ± 1.5 nm, respectively) and spherical in shape (Fig. S8).

To confirm the homogeneous dispersion of metal NPs in the WF, HAADF-STEM and EDX analyses have been carried out on H-Pd/WF (Fig. 5, top) and H-Rh/WF (Fig. 5, bottom) samples. As demonstrated by the images, EDX showed that, in both cases, metals were homogeneously dispersed in the wool support and no aggregations were evident.

The XPS spectra of Pd and Rh NPs are displayed in Fig. 6. The spectra of both elements required more than one component to be properly fitted, indicating, overall, the presence of multiple species of these elements at the surface. Due to spin–orbit

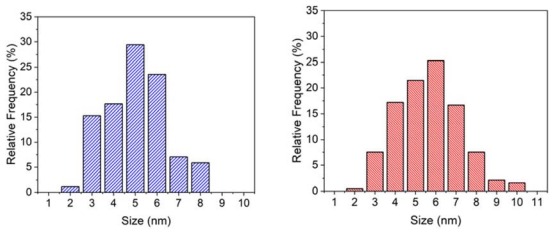

Fig. 4 Diameter sizes (nm) of H-Pd/WF (left) and H-Rh/WF (right).

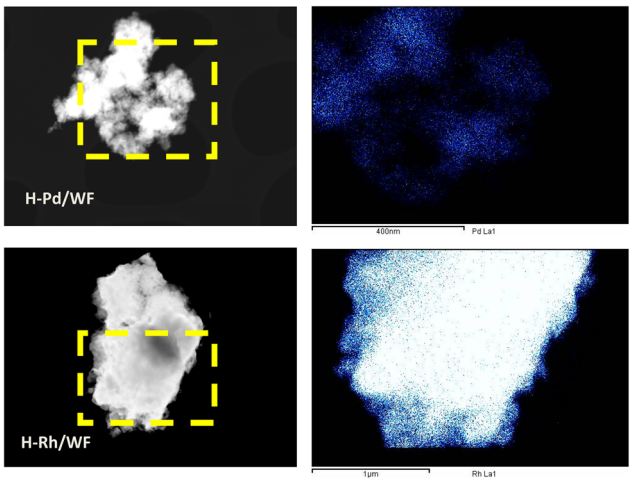

Fig. 5 EDX compositional mapping analysis for H-Pd/WF (upper) and H-Rh/WF (bottom) samples.

coupling, the 3d core transition returned a doublet: Pd $3d_{3/2}$ and Pd $3d_{5/2}$. In particular, the spectrum of palladium in the H-Pd/WF sample required the use of three separate doublets located at different energies. Higher is the energy value (binding energy, BE), the more oxidated is the chemical species responsible for such signal. So, the peak located at lower BE value (335.0 ± 0.1 eV, blue area in Fig. 6 top) was attributable to metallic palladium (Pd^0); the one at intermediate value (337.7 ± 0.1 eV, green area in Fig. 6 top) was attributable to PdO, and the one located at higher BE value (339.7 ± 0.1 eV, purple area in Fig. 6 top) was consistent with the presence of highly oxidized palladium oxides (PdO_2).

In L-Pd/WF sample, the peaks attributable to Pd^{2+} and Pd^{4+} were still present while the peak attributable to metallic palladium was neglectable. Indeed, spectra, collected on the same sample after Ar-sputtering, displayed the presence of metallic palladium under spectra fitting, based upon the position of the peaks neath.

Similar behavior characterizes the L-Rh/WF and H-Rh/WF samples. In this case, only two doublets (Rh $3d_{5/2}$ e Rh $3d_{3/2}$), accounting for rhodium in different chemical environments, need to be employed to fit the experimental data. On the ground of the BE value, these components can be attributed to metallic Rh (306.3 ± 0.1 eV, blue area in Fig. 6 bottom) and rhodium oxide (Rh_2O_3, 309.4 ± 0.1 eV, green area in Fig. 6 bottom).

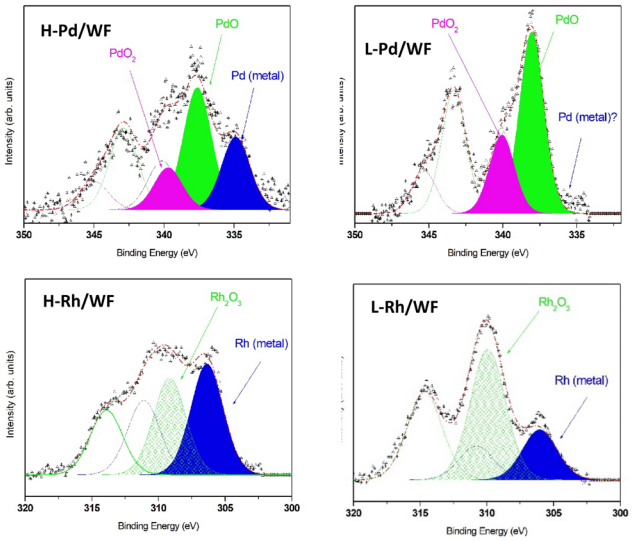

Fig. 6 High resolution XPS spectra of palladium (top) and rhodium (bottom) characteristic peaks collected on metal NPs/WF. Scatter lines represent experimental data; solid and dash lines represent the contributions and envelope spectra. Filled areas represent the $3d_{3/2}$ peaks of palladium and rhodium different chemical species.

Resuming their characteristics, Pd/WF and Rh/WF were spherical in shape, similar in size, both at high and at low concentration.

Firstly, metal NPs/WF were tested as catalysts in the hydrogenation reaction of MA, carried out in batch, in water solution at room temperature, under H_2 flux or in presence of aqueous hydrazine sulfate as reducing agent (Fig. 7).

Successful results were observed in the presence of H_2 for H-Pd/WF and H-Rh/WF: employing 3% of metal/MA molar ratio, a quantitative conversion and a full selectivity to SA were obtained in 2 h (Table 2). No by-products were observed in ^1H NMR spectra (Fig. S9–S13). The trend of the turnover numbers (TON, Tables S1 and S2) indicates similar courses for both catalysts, raising a value of about 60 (mol of product/mol of metal) after 2 h of reaction, modest but promising results, considering also these mild conditions. Turnover frequency values (TOF), shown in Tables S1 and S2, suggest that the initial stage of the catalysts' activity (about 30 minutes) was steady. Then an intense conversion of MA to SA was observed and, after one hour, the reaction slowed down ending in 2 h. The catalytic behavior of the H-Pd/WF and of the H-Rh/WF appeared similar under flux of H_2 gas. TOF values of Pd catalyst appeared lower than those reported in literature, but a real assessment is not easy because the published data referred to different reaction conditions (higher temperature, use of formic acid, alcoholic

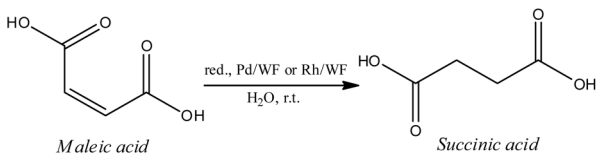

Fig. 7 The reduction reaction of MA to SA.

Table 2 Conversions of MA and yields of SA (mol%) in batch reactions, carried out in the presence of the catalysts (3% mol of metal/mol of MA) in water solution at room temperature and under H_2 flux

Catalyst	Reaction time (h)	MA conversion (mol%)	SA yield (mol%)
H-Pd/WF	1	70	70
	2	100	100
H-Rh/WF	1	70	70
	2	97	97

Table 3 Conversions of MA and yields of SA (mol%) in batch reactions, carried out in the presence of the recycled catalysts in water solution at room temperature and under H_2 flux

Catalyst	Reaction cycle number	Reaction time (h)	MA conversion (mol%)	SA yield (mol%)
H-Pd/WF	1	2	100	100
	2	2	100	100
	3	2	100	100
	4	2	100	100
	5	2	100	100
H-Rh/WF	1	2	97	97
	2	2	97	97
	3	2	97	97
	4	2	97	97
	5	2	97	97

solvents), and to different catalysts (*e.g.*, Pd on inorganic oxides). TOF Rh catalysts were not reported for this hydrogenation reaction.[41,42]

The reactions were conducted even in the presence of L-Pd/WF and L-Rh/WF; in these cases, the conversion was slower reaching 100% only after 24 h; the selectivity was quantitative again (Fig. S14 and S15).

The catalysts were easily separated from aqueous solution by filtration on a paper filter, and water washed to reuse them. Recycle tests were performed in the presence of H-Pd/WF and H-Rh/WF showing no loss of catalytic activity up to 5 cycles (Table 3). A partial leaching of the metals from the WF was observed with a loss of 38% of Pd and 25% of Rh only after 5 cycles of hydrogenation (Table 4).

Hydrazine sulfate was tested as an alternative reducing agent to eliminate the need for gaseous reagents and allow to perform

Table 4 Amounts of Pd and Rh detected by ICP analysis at WF catalysts before the hydrogenation reaction and after 1 or 5 cycles of reaction under H_2 flux

Catalyst	After reaction cycle number	Metal supported on WF (%, w/w)
H-Pd/WF	0	100
	1	92
	5	62
H-Rh/WF	0	100
	1	78
	5	75

Table 5 Conversions of MA and yields of SA (mol%) in batch reactions, carried out in the presence of hydrazine sulfate and H-Pd/WF or H-Rh/WF (15% mol of metal/mol of MA), in water solution at room temperature

Catalyst	Reaction time (h)	MA conversion (mol%)	SA yield (mol%)
H-Pd/WF	24	0	0
H-Rh/WF	1	2	2
	3	30	30
	5	44	44
	24	48	48

reactions even in a home-made fixed-bed continuous reactor. In preliminary batch experiments, the H-Pd/WF catalyst proved ineffective with hydrazine salt, resulting in no detectable conversion of MA, even at a 15% metal/MA molar ratio (Fig. S16). In contrast, a moderate activity in batch of the H-Rh/WF catalyst was observed (48% conversion after 24 h, Fig. S17), employing 15% metal/MA molar ratio. Notably, the reaction was fully selective for SA production, demonstrating the potential of Rh-based catalysts in selective hydrogenation processes, albeit with reduced efficiency under these conditions (Table 5).

We recovered and reused the catalyst after washing, also in these conditions. We observed 28% of MA conversion during the second cycle and 20% in the fifth one but maintaining full selectivity.

Building on the promising batch results with hydrazine sulfate and H-Rh/WF, a fixed-bed reactor was designed, using a repurposed HPLC column (10 cm length, 2 mm internal diameter, 63 μL reactor volume, Fig. S18) to perform the reaction in continuous-flow mode. The old silica stationary phase was mechanically removed, and the empty metal tube was filled with L-Rh/WF or L-Pd/WF catalysts.

Various flow rates of the aqueous solution were tested, reaching up to 500 μL h^{-1} without encountering back-pressure issues. The optimal flow rate to ensure sufficient residence time (75 minutes) for complete reagent conversion (with 100% selectivity, Fig. S19) was 52 μL h^{-1} when using the L-Rh/WF catalyst (Table 6). Increasing the flux up to 205 μL h^{-1}, a 72% of MA conversion was obtained after only 19 minutes rather than 75 minutes, necessary for 100% conversion.

This setup demonstrated the feasibility of conducting this hydrogenation reaction selectively in a continuous-flow system with hydrazine salt as the reducing agent. In fact, even L-Pd/WF

Table 6 Conversions of MA and yields of SA and FA (mol%), carried out in a fixed-bed reactor in the presence of the catalysts and hydrazine sulfate, in water solution at room temperature

Catalyst	Residence time (min)	MA conversion (mol%)	SA yield (mol%)	FA yield (mol%)
L-Pd/WF	180	59	38	20
L-Rh/WF	19	72	57	15
	38	86	76	10
	75	100	100	0

catalyst was active in flow-mode, converting 59% of MA to 38% of SA and 20% of FA in 180 minutes (Table 6 and Fig. S20). Using L-Rh/WF, the catalyzed isomerization of MA to FA was observed only when the conversion of the substrate was not complete (up to 38 minutes, Fig. S21 and S22).

Discussion

The morphology of these catalysts, as NPs supported on WF, can be the key to their activity.[6] The homogeneous dispersion and the size of the metal NPs on the surface of the WF is crucial to maximize the surface area of the catalyst and, therefore, its activity and selectivity.

SEM images and HAADF-STEM analysis, together with EDX mapping, showed that the metal NPs were homogeneously dispersed in the wool support with no apparent aggregation. TEM micrographs showed that the Pd and Rh NPs were spherical, small, and embedded in the WF. Such small particles (about 5 nm) greatly increased the contact area between the catalyst and the substrate, dramatically affecting the reaction rate. XRD diffractograms and XPS spectra showed the presence of multiple species of Pd and Rh on the surface of the fibers. This suggests that the metals were present in a mixture of oxidation states including Pd^0, Pd^{2+}, Pd^{4+}, Rh^0, and Rh^{3+}. The presence of higher oxidation states is probably due to the surface oxidation of these NPs, based even on the XRD results showing the metal cores.

Likewise, the use of WF, as a natural and biodegradable support, eliminates the need for NPs stabilizers, adding a significant advantage in terms of sustainability. Furthermore, WF can be considered an appropriate active support for noble metal catalysts, at least in the aqueous hydrogenation reactions of MA; in the literature, the catalytic activity of Pd NPs for the hydrogenation of MA has been reported to vary significantly, depending on the nature of the support material.[35]

Pd/WF and Rh/WF demonstrated to fully reduce the C=C in the presence of gaseous H_2 and to be recovered and reused, at least, for 5 cycles. In fact, the observed metal leaching did not affect catalytic activity until the loss became significant.

The behavior with hydrazine sulfate was different, mainly due to the necessary step of its decomposition to hydrogen gas.[43] H-Rh/WF catalyst demonstrated moderate activity with hydrazine sulfate in batch reactions but excellent results in flow-mode. The observed increase in MA conversion and SA yield, when transitioning from batch to continuous-flow conditions, can be attributed to several factors, such as enhanced mass transfer phenomena, more efficient surface interactions between the substrate and catalyst, a higher catalyst-to-reagent ratio, and an extended catalyst lifetime under flow conditions.[44,45]

Interestingly, the Pd/WF catalyst showed no detectable activity with hydrazine sulfate in batch but 59% of MA conversion in flow system, underlining a significant difference in reactivity between rhodium and palladium under these conditions. This observation suggests that rhodium's superior capability to decompose hydrazine facilitates the transfer of hydrogen to the substrate. In literature, the efficacy of bulk Rh and of the supported Rh catalysts is well documented, even at temperatures <100 °C; Pd catalysts are very active compared to other transition metals but are less efficient than Rh catalysts.[43,46–48] Both metals, as reported, are selective for the conversion of hydrazine to hydrogen (and nitrogen, of course).

Metals leaching is more likely pronounced in batch reactions, where is even due to the lower mechanical stress on the catalysts (*e.g.*, magnetic stirrer).[49] It was reported that the wool-supported Pd NPs catalyst is fragile and can be damaged by the mechanical stirrer.[6]

Hydrazine sulfate was employed as an alternative hydrogen source to gaseous H_2, by eliminating the need for pressurized gases. Despite the fact that hydrazine is harmful and toxic to humans and its use poses risks for environment, especially aquatic organisms,[50] its salts are less hazardous due to lower volatility, easier to manipulate, and non-explosive character. The objective of this first test was essentially to verify the activity of the new catalysts. Hydrazine sulfate was used essentially to have a water-soluble compound as an easy source of hydrogen.

Both prepared Pd/WF and Rh/WF catalysts were able to reduce MA to SA selectively by adsorbing hydrogen and transferring it only to the double bond of MA. Rh/WF exhibited a slightly higher activity (*i.e.*, in flow experiments), likely due to its affinity for π-bond activation and, in the case, for hydrazine decomposition to hydrogen.[51]

Compared to the literature examples, such as Pd NPs supported on synthetic polymers or on oxides, Pd/WF and Rh/WF catalysts showed superior (or analogous) conversion and selectivity but using milder conditions (*e.g.*, room temperature, atmospheric pressure).[30,34,36]

Indeed, the catalyst activity is the main property and issue for the researchers but, from an industrial point of view, the selectivity and the productivity, also related to catalyst lifetime, are very important.[34,52] The reactor productivity with L-Rh/WF, calculated as [$mmol_{SA}/(mmol_{catalyst} \times$ reactor mL $\times$ h)], was 0.3 for the experiments in which full conversion was pursued, while it increased to 1.7 using a flow rate of 500 μL h^{-1} and so decreasing MA conversion to 60%.

In our conditions, the life of packed bed reactor was usually 12 weeks: no loss of conversion or selectivity was observed for both catalysts. In the following working period (up to 10 weeks), without any regeneration of the packed bed, the conversion was reduced to 62% with L-Rh/WF and to 34% with L-Pd/WF but always with 100% selectivity.

Experimental

Materials

$RhCl_3 \cdot 3H_2O$ was purchased by Johnson & Johnson Innovative Medicine, $PdCl_2$ by Strem Chemicals, and the other reagents by Carlo Erba Reagents and Merck. Low-grade wool, a mix of waste and used WF, was a gift from a local textile manufacturer.

Synthesis and characterization of Pd NPs/WF and Rh NPs/WF

The low-grade wool was washed with water, frozen in liquid N_2 for 20 minutes and cut with scissors; WF with a size smaller

than 250 μm were selected by a sieve and used to prepare the metal NPs/WF.

Pd NPs/WF was synthesized mixing 0.1 g of WF with 0.071 g (H-Pd NPs/WF) or 0.035 g (L-Pd NPs/WF) of $PdCl_2$ in 10 mL of water and 450 μL or 270 μL of formic acid, respectively. The mixture was stirred at 80 °C for 6 h. Then Pd NPs/WF, turned black, was filtered on paper, carefully washed with water, and dried at 60 °C for 15 minutes without color changes.

Rh NPs/WF was synthesized mixing 0.1 g of WF with 0.105 g (H-Rh NPs/WF) or 0.052 g (L-Rh NPs/WF) of $RhCl_3 \cdot 3H_2O$ in 10 mL of water and 450 μL or 270 μL of formic acid, respectively. The mixture was stirred at 80 °C for 6 h. Then Rh NPs/WF, turned dark brown, was filtered on paper, carefully washed with water, and dried at 60 °C for 15 minutes without color changes.

The specific concentrations (w/w %) were 43% Pd (H-Pd NPs/WF), 41% Rh (H-Rh NPs/WF), 21% Pd (L-Pd NPs/WF), and 20% Rh (L-Rh NPs/WF). The catalysts were characterized by SEM, TEM, EDX, XRD, XPS.

All syntheses were repeated in the absence of formic acid for comparison purposes.

Scanning electron microscope (SEM) images were acquired by scanning electron microscopy Zeiss Sigma 300 FE equipped with Bruker Quanta EDX detector. The samples were put on aluminum stubs and they were attached with double-sided conductive carbon pads; over them a conductive chromium film was deposited by metallizer Quorum mod. Q150T-ES.

Transmission electron microscope (TEM) analyses of the samples were carried out with a ZEISS LIBRA 200FE HRTEM instrument, equipped with a FEG source operating at 200 kV, in column second generation omega filter, HAADF STEM facility, EDS probe for chemical analysis. The samples were ultrasonically dispersed in 2-propanol and a drop of the obtained solution was deposited on a holey-carbon film supported on a copper TEM grid (300 mesh). More than 100 NPs were measured to estimate the nanoparticle sizes using iTEM (TEM Imaging Platform Olympus) and the mean particle diameter (d_m) was calculated by using the formula $d_m = \sum d_i n_i / \sum n_i$, where n_i is the number of particles with diameter d_i. EDX spectra and element maps were collected along with HAADF-STEM micrographs.

X-ray diffraction (XRD) analysis was performed on a Miniflex II Rigaku automated powder XRD system (Cu Kα radiation, 45 kV, 100 mA) (RINT 2500, Japan). Diffraction data were recorded using continuous scanning at 3° min^{-1}, with 0.010° steps.

X-ray photoelectron spectroscopy (XPS) measurements were performed using a non-monochromated Mg-Ka X-ray source (1254.6 eV) and a VSW HAC 5000 hemispherical electron energy analyzer. Photoelectron spectra were acquired in the constant-pass-energy mode at $E_{pas} = 22$ eV, and the overall energy resolution was 1.2 eV measured as a full-width at half maximum (FWHM) of the Ag $3d_{5/2}$ line of a pure silver reference. The spectra energy scale was referred to the 1s peak of organic carbon and the spectra were fitted using XPSPeak 4.1 software employing Gauss–Lorentz curves to fit the data after subtraction of a Shirley-type background.

The total Pd or Rh content was measured by an Inductively coupled plasma (ICP) apparatus (Varian 720-ES Series) prior acidification of the liquid samples with concentrated HNO_3. The resulting solutions were then collected in 10 mL volumetric flasks with ultrapure water and then analyzed by an ICP instrument. For the solid samples, 20 mg of the catalyst was mixed with 10 mL of HCl 12 M on a beaker with boiling water until complete dissolution. The resulting solutions were then collected in 50 mL volumetric flasks with ultrapure water and then analyzed by ICP instrument. Concentrations of samples were adjusted with HNO_3 2% v/v in order to be within the concentration range of the calibration straight, that was built in the 0.1–100 μg L^{-1} range, starting from S standard solution of 100 μg L^{-1}. Measurements were carried out with a wavelength of 182 nm.

Hydrogenation reactions in batch mode

In the hydrogenation of MA with gaseous H_2, 0.280 g of MA (2.4 mmol, 0.24 M) and 0.02 g of H-Pd NPs/WF (0.08 mmol Pd; 3% Pd/MA mol mol^{-1}) or 0.02 g of H-Rh NPs/WF (0.08 mmol Rh; 3% Rh/MA mol mol^{-1}) in 10 mL of water were stirred in a flask at room temperature (about 20 °C) under H_2 flux for 24 h. The reactions were performed even with L-Pd NPs/WF (or L-Rh NPs/WF) catalyst: in this case, 0.04 g were used keeping the metal/reagent ratios unchanged.

In the hydrogenation of MA in the presence of hydrazine sulfate as reducing agent, 0.17 g of MA (1.5 mmol, 0.03 M) with 0.38 g of hydrazine sulfate (3 mmol, 0.06 M) in the presence of 0.001–0.056 g of H-Pd NPs/WF (or H-Rh NPs/WF, both 0.2–60 mmol metal; 5–15% % metal/MA mol mol^{-1}) catalyst in 50 mL of water were stirred in a flask at room temperature (about 20 °C) for 24 h.

Hydrogenation reactions in continuous-flow mode

The continuous-flow experiments were conducted using a syringe pump 11 Plus Manual from Harvard Apparatus (single syringe; flow rate: 0.0014 μL h^{-1}–26.56 μL min; accuracy: ±0.5%) connected with a spent HPLC column (10 cm length, 2 mm internal diameter), cleaned and packed with 0.1 g of L-Pd NPs/WF or L-Rh NPs/WF. Its internal volume was experimentally calculated (63 μL volume) measuring the reaction solvent fluxed into the packed column.

At first, the reactor was dried fluxing a light air stream with a syringe pump, then the water reaction mixture containing MA (0.07 M) and hydrazine sulfate (0.05 M) was pumped inside the column at the established flow rate in the range 25–300 μL h^{-1}. The collected solution at the end of the column was analyzed as it is by ^1H NMR.

NMR analysis

The identification of the products, the conversion of the reagents and the yields of products were monitored by ^1H NMR.[24,31,53,54]

Nuclear magnetic resonance spectrometer was a Bruker Avance 300 (7.05 tesla) equipped with a high resolution multinuclear probe operating in the range of 30–300 MHz. The

sample was analyzed as it, in aqueous solution; to eliminate the dominant water signal in the ^{1}H NMR spectra (δ around 4.7 ppm), water suppression was carried out using a presaturation sequence of a composite pulse (zgcppr, Bruker sequence). A co-axial capillary tube that contained a 30 mM D_2O solution of 3-(trimethylsilyl) propionic-2,2,3,3-d_4 acid, sodium salt, was used as the reference both for the lock procedure and for the quantitative analysis.

Peak assignments were confirmed by comparison with commercial MA, FA and SA in water solution; these compounds have unique ^{1}H chemical shift, water solubility, stability, and accurate NMR areas since they were proposed as standards for quantitative NMR analysis.[55]

Before monitoring any reaction, the calibration curves were built by ^{1}H NMR, using commercial MA, FA and SA in water solutions at known concentrations. To ensure quantitative reliability, calibration curves were constructed for MA ($\delta = 6.3$ ppm), FA ($\delta = 6.8$ ppm), and SA ($\delta = 2.6$ ppm) by plotting the integrated peak areas against the known concentrations over the range employed in the experiments. In all cases, a linear correlation was obtained, with regression lines of the type: $A = m \cdot C + b$, where A is the integrated peak area and C is the molar concentration. The calibration curves exhibited excellent linearity, with coefficients of determination (R^2) > 0.99, confirming that peak integration could be used for accurate quantification.

Conclusions

WF were successfully repurposed as sustainable supports for Pd and Rh NPs, enabling selective hydrogenation of MA to SA under mild aqueous conditions. The catalysts displayed excellent activity and complete selectivity in batch reactions with gaseous hydrogen, maintaining performance after multiple recycling cycles and showing only partial metal leaching.

In continuous-flow experiments, Rh NPs/WF achieved complete conversion within 75 minutes using hydrazine sulfate as hydrogen donor, while Pd NPs/WF showed moderate activity. The higher efficiency observed under flow demonstrates the advantages of fixed-bed operation, including the raising of the catalyst lifetime, and stable performance over several weeks. These results indicate that wool-supported catalysts can be effectively integrated into flow reactors, offering both sustainability in catalyst preparation and operational benefits in process intensification.

Overall, the study confirms the potential of waste wool as an inexpensive, biodegradable support for transition metal catalysts.

The combination of wool-supported metal NPs with continuous-flow technology represents a promising pathway towards greener hydrogenation processes, with future efforts directed to replacing hydrazine salt with safer and greener hydrogen sources (*e.g.*, formic acid) and extending the methodology to other reactions of industrial relevance.

Author contributions

F. C., methodology, investigation, writing – original draft; A. M., investigation, data curation; S. C., resources, formal analysis, writing – original draft; L. P., resources, formal analysis, writing – original draft; A. P., conceptualization, writing – review & editing; C. D. N., resources, formal analysis, writing – original draft; L. T., conceptualization, writing – review & editing, supervision; N. d'A., funding acquisition, conceptualization, writing – review & editing.

Conflicts of interest

There are no conflicts to declare.

Data availability

The data supporting this article have been included as part of the supplementary information (SI). Supplementary information is available. See DOI: **https://doi.org/10.1039/d5ra05365j**.

Acknowledgements

The research project was partially supported by the FSE-REACTEU, PON Ricerca e Innovazione 2014–2020 DM 1062/2021, Cod: MUR 53-G-14753. N. d'A., L. T., F. C., A. M. express their gratitude to the CAST – Center for Advanced Studies and Technology of University "G. d'Annunzio" for supplying the cryogenic gases. N. d'A., L. T., F. C., A. M. thank INGENIUM Alliance of European Universities (ERASMUS-EDU-2022-EUR-UNIV-2, project number 101090042) for the support. A. P. gratefully acknowledges support from the RETURN Extended Partnership, funded by the European Union through the Next-GenerationEU program (National Recovery and Resilience Plan – NRRP, Mission 4, Component 2, Investment 1.3 – D.D. 1243 2/8/2022, PE0000005).

References

1 S. J. McNeil, M. R. Sunderland and S. J. Leighs, *Appl. Catal., A*, 2017, **541**, 120–140.
2 Y. Zhang, W. Wang and S. Li, *Asian J. Chem.*, 2015, **27**, 111–116.
3 Y. Y. Yao, W. X. Chen and S. S. Lu, *J. Appl. Polym. Sci.*, 2006, **102**, 4378–4382.
4 A. Shaabani, Z. Hezarkhani and E. Badali, *RSC Adv.*, 2015, **5**, 61759–61767.
5 Q. Yang, Z. Quan, B. Du, S. Wu, P. Li, Y. Sun, Z. Lei and X. Wang, *Catal. Sci. Technol.*, 2015, **5**, 4522–4531.
6 S. Ghadamgahi, J. H. Johnston and C. Fonseca-Paris, *Nanomaterials*, 2018, **8**, 1–12.
7 A. Krastanov, *Appl. Microbiol. Biotechnol.*, 1997, **47**, 476–481.
8 J. V. Edwards, N. T. Prevost, B. Condon, A. French and Q. Wu, *Cellulose*, 2012, **19**, 495–506.
9 Q. Wang, X. Fan, Y. Hu, J. Yuan, L. Cui and P. Wang, *Bioprocess Biosyst. Eng.*, 2009, **32**, 633–639.
10 Eurostat, Eurostat Data, **https://ec.europa.eu/eurostat/en/**.
11 European Parliament and Council, *Off. J. Eur. Union*, 2009, **300**, 1–33.
12 E. Reichelt, M. P. Heddrich, M. Jahn and A. Michaelis, *Appl. Catal., A*, 2014, **476**, 78–90.

13 J. Zhang, Y. Li, J. Li, Z. Zhao, X. Liu, Z. Li, Y. Han, J. Hu and A. Chen, *Powder Technol.*, 2013, **246**, 356–362.
14 H. Gong, H. Zhou, R. Forrest, S. Li, J. Wang, J. Dyer, Y. Luo and J. Hickford, *Genes*, 2016, **7**, 24.
15 J. McKittrick, P. Y. Chen, S. G. Bodde, W. Yang, E. E. Novitskaya and M. A. Meyers, *Jom*, 2012, **64**, 449–468.
16 J. H. Bradbury and V. G. Kulkarni, *Text. Res. J.*, 1975, **45**, 79–83.
17 A. Körner and V. K. Naithani, *J. Text. Inst.*, 1999, **90**, 14–18.
18 J. W. Rowen and R. L. Blaine, *Ind. Eng. Chem.*, 1947, **39**, 1659–1663.
19 M. Rehan, H. M. Mashaly, A. S. Montaser and R. M. Abdelhameed, *J. Mol. Liq.*, 2023, **387**, 122603.
20 Y. Song, N. Qi, K. Li, D. Cheng, D. Wang and Y. Li, *RSC Adv.*, 2022, **12**, 8108–8118.
21 A. Shaabani and Z. Hezarkhani, *Appl. Organomet. Chem.*, 2017, **31**, e3542, DOI: **10.1002/aoc.3542**.
22 A. Shaabani, Z. Hezarkhani and M. T. Faroghi, *Monatsh. Chem.*, 2016, **147**, 1963–1973.
23 J. Wegner, S. Ceylan and A. Kirschning, *Chem. Commun.*, 2011, **47**, 4583–4592.
24 L. Tonucci, A. Mascitti, A. M. Ferretti, F. Coccia and N. d'Alessandro, *Catalysts*, 2022, **12**, 1–14.
25 K. Di Pietrantonio, F. Coccia, L. Tonucci, N. D'Alessandro and M. Bressan, *RSC Adv.*, 2015, **5**, 68493–68499.
26 F. Coccia, L. Tonucci, N. D'Alessandro, P. D'Ambrosio and M. Bressan, *Inorg. Chim. Acta*, 2013, **399**, 12–18.
27 F. Coccia, L. Tonucci, P. Del Boccio, S. Caporali, F. Hollmann and N. D'Alessandro, *Nanomaterials*, 2018, **8**, 853.
28 F. Coccia, L. Tonucci, D. Bosco, M. Bressan and N. d'Alessandro, *Green Chem.*, 2012, **14**, 1073–1078.
29 J. H. Schrittwieser, F. Coccia, S. Kara, B. Grischek, W. Kroutil, N. D'Alessandro and F. Hollmann, *Green Chem.*, 2013, **15**, 3318.
30 B. Ye, S. Sun, H. Wang, H. Huang, M. U. Rehman, X. Sun, Y. Xu and Y. Zhao, *Res. Chem. Intermed.*, 2023, **49**, 4443–4459.
31 F. Coccia, A. Mascitti, G. Rastelli, N. D'Alessandro and L. Tonucci, *Appl. Sci.*, 2025, **15**, 1631.
32 Y. Rodenas, R. Mariscal, J. L. G. Fierro, D. Martín Alonso, J. A. Dumesic and M. López Granados, *Green Chem.*, 2018, **20**, 2845–2856.
33 J. S. Kim, J. H. Baek, Y. B. Ryu, S. S. Hong and M. S. Lee, *J. Nanosci. Nanotechnol.*, 2015, **15**, 290–294.
34 A. Orozco-Saumell, R. Mariscal, J. Iglesias, P. Maireles-Torres and M. López Granados, *Sustain. Energy Fuels*, 2022, **6**, 5160–5176.
35 M. A. Kulagina, E. Y. Gerasimov, T. Y. Kardash, P. A. Simonov and A. V. Romanenko, *Catal. Today*, 2015, **246**, 72–80.
36 M. Y. Byun, J. S. Kim, J. H. Baek, D. W. Park and M. S. Lee, *Energies*, 2019, **12**, 3–10.
37 Q. Wang, Y. Wang, P. Guo, Q. Li, R. Ding, B. Wang, H. Li, J. Liu and X. S. Zhao, *Langmuir*, 2014, **30**, 440–446.
38 B. Xu, M. Niu, L. Wei, W. Hou and X. Liu, *J. Photochem. Photobiol., A*, 2007, **188**, 98–105.
39 L. Xu, X.-C. Wu and J.-J. Zhu, *Nanotechnology*, 2008, **19**, 305603.
40 T. Aaltonen, M. Ritala and M. Leskelä, *Electrochem. Solid-State Lett.*, 2005, **8**, 3–6.
41 M. A. Kulagina, P. A. Simonov, E. Y. Gerasimov, R. I. Kvon and A. V. Romanenko, *Colloids Surf., A*, 2017, **526**, 29–39.
42 A. Orozco-Saumell, M. Retuerto, A. C. Alba-Rubio, P. Maireles-Torres, J. Iglesias, R. Mariscal and M. López Granados, *J. Catal.*, 2024, **439**, 115780.
43 V. A. Matyshak and O. N. Silchenkova, *Kinet. Catal.*, 2022, **63**, 339–350.
44 R. Porta, M. Benaglia and A. Puglisi, *Org. Process Res. Dev.*, 2016, **20**, 2–25.
45 F. M. Akwi and P. Watts, *Chem. Commun.*, 2018, **54**, 13894–13928.
46 P. Adamou, S. Bellomi, E. Harkou, X. Chen, J. J. Delgado, N. Dimitratos, G. Manos, A. Villa and A. Constantinou, *Chem. Eng. J.*, 2024, **493**, 152715.
47 R. Maurel, *J. Catal.*, 1978, **51**, 293–295.
48 P. C. Pandey, S. Shukla and Y. Pandey, *J. Mater. Res.*, 2017, **32**, 3574–3584.
49 R. P. Jumde, C. Evangelisti, A. Mandoli, N. Scotti and R. Psaro, *J. Catal.*, 2015, **324**, 25–31.
50 World Health Organization, *Hydrazine, EHC*, 1987, vol. 68, pp. 1–62.
51 S. K. Singh, X.-B. Zhang and Q. Xu, *J. Am. Chem. Soc.*, 2009, **131**, 9894–9895.
52 S. L. Scott, *ACS Catal.*, 2018, **8**, 8597–8599.
53 S. K. Bharti and R. Roy, *Trac. Trends Anal. Chem.*, 2012, **35**, 5–26.
54 S. Dutta, L. Wu and M. Mascal, *Green Chem.*, 2015, **17**, 2335–2338.
55 G. A. Nagana Gowda, N. N. Hong and D. Raftery, *Anal. Chem.*, 2021, **93**, 3233–3240.